CrystEngComm

PAPER

View Article Online
View Journal | View Issue

Check for updates

Cite this: *CrystEngComm*, 2024, **26**, 4278

Controllable growth of large-size α-GeTe nanosheets with ferroelectricity by substrate pre-annealing†

Zhaxi Suonan,[ab] Shuo Mi,[ab] Hanxiang Wu,[ab] Hua Xu,[ab] Haoyan Zhang,[ab] Shanshan Chen,[ab] Zhihai Cheng[ab] and Fei Pang*[ab]

Received 17th May 2024,
Accepted 10th July 2024

DOI: 10.1039/d4ce00499j

rsc.li/crystengcomm

The atmospheric chemical vapor deposition (APCVD) method has been widely applied to synthesize high-quality two-dimensional materials. GeTe has many intriguing properties, such as phase transition, thermoelectric and ferroelectricity, which allow unique opportunities for functional ferroelectric devices. Here, we systematically investigated effects of various parameters during the growth of α-GeTe nanosheets on mica by APCVD. Single-crystal α-GeTe nanosheets possess a lateral size of up to ~30 μm and a thickness as low as ~8.6 nm. It was found that substrate pre-annealing significantly impacted the nucleation density of α-GeTe nanosheets. Furthermore, the room-temperature ferroelectric properties of α-GeTe nanosheets grown by CVD are reported for the first time. This work offers an effective accessible method for the controllable growth of large-size 2D α-GeTe to explore its fascinating multiferroic properties.

Published on 11 July 2024. Downloaded on 11/19/2024 1:20:51 PM.

1. Introduction

As a new family of two-dimensional (2D) materials, group IVA–VIA semiconducting materials[1] have attracted tremendous attention. As a narrow-band-gap semiconductor, GeTe has many interesting physical properties such as phase change properties,[2–6] thermoelectricity,[7,8] and Rashba spin splitting.[9–11] For the ferroelectricity can persist in the nanoscale GeTe films,[12] GeTe would be applied in nonvolatile memory elements. Although ferroelectric bulk materials have been studied in the past and are widely utilized in practical devices, ferroelectric properties of 2D GeTe, especially those fabricated by CVD, are less reported. Ferroelectric features make 2D GeTe (ref. 13–15) a promising candidate for high-capacity and high-density ferroelectric devices.[16,17] Therefore, the preparation of 2D α-GeTe has become important for nanoscale devices such as non-volatile memory.

Chemical vapor deposition (CVD) is considered a potential method to synthesize large-area high-quality 2D materials,[18,19] which can be adjusted by modifying various parameters such as the substrate,[20,21] source-substrate distance,[22] carrier gas[23] and growth temperature. According to previous reports,[18] GeTe compounds possess three phases, namely, α-GeTe, β-GeTe, and γ-GeTe, showing great potential in phase change memory devices. Among them, α-GeTe is stable at room temperature. Although several researchers have successfully fabricated α-GeTe nanosheets by CVD,[18] the controllable growth of α-GeTe and its ferroelectric properties are still a challenge. The role of various parameters, especially substrate pre-annealing, during the growth of α-GeTe is yet to be systematically investigated.

Herein, we report the growth of 2D α-GeTe nanosheets by an atmospheric pressure CVD (APCVD) on a mica substrate by adjusting several growth parameters, including substrate pre-annealing, growth time and temperature. The resulting α-GeTe nanosheets are hexagonal and triangular, with a thickness of 8.6 nm. It is found that substrate annealing in air and growth temperature are the key parameters to control the growth of GeTe. Substrate pre-annealing is effective in reducing the density of nucleation and promoting the lateral growth of α-GeTe nanosheets. The GeTe nanosheets display high-quality single crystals with α phase, which was confirmed by X-ray diffraction (XRD). Furthermore, the ferroelectric properties of the α-GeTe nanosheets are measured using piezoresponse force microscopy (PFM). To

[a] *Beijing Key Laboratory of Optoelectronic Functional Materials & Micro-nano Devices, Department of Physics, Renmin University of China, Beijing 100872, China. E-mail: feipang@ruc.edu.cn*
[b] *Key Laboratory of Quantum State Construction and Manipulation (Ministry of Education), Renmin University of China, Beijing, 100872, China*

† Electronic supplementary information (ESI) available. See DOI: https://doi.org/10.1039/d4ce00499j

This journal is © The Royal Society of Chemistry 2024

Published on 11 July 2024. Downloaded on 11/19/2024 1:20:51 PM.

the best of our knowledge, this is the first report on ferroelectric properties of CVD-grown GeTe nanosheets.

2. Experimental section

2.1 Growth of α-GeTe nanosheets

α-GeTe nanosheets were synthesized on mica substrates using a one-zone tubular furnace under atmospheric pressure. As shown in Fig. 1(a) 10 mg GeTe powder (purity 99.999%, 3A) was placed at the center of the tube furnace, and mica substrates were placed downstream at ~10 cm away from GeTe powders. Before the heating process, the system was flushed with ultrahigh purity Ar. The freshly cleaved mica substrate was annealed in air at 300 °C for 1 h and then the furnace was naturally cooled down to room temperature. During the growth process of GeTe nanosheets, the single-zone tube furnace was heated up to 600 °C within 20 min. The temperature was maintained for 10 min with a constant flow of 200 sccm Ar for the growth of α-GeTe. Once the heating process ended, the sample was cooled to 500 °C under 300 sccm Ar, and then quickly cooled to room temperature.

2.2 Characterization

The morphology of α-GeTe nanosheets was characterized by optical microscopy (OM, 6XB-PC) and atomic force microscopy (AFM, Bruker Dimension icon). The crystalline phase was characterized by X-ray diffraction (XRD, Bruker D8 Advance) with Cu K_α radiation, Raman spectroscopy (Alpha 300R, WITec) with a 532 nm laser as the excitation source, scanning electron microscopy (SEM, FEI NOVA NANOSEM 450) with an energy dispersive spectrometer (EDS), X-ray photoelectron spectroscopy (XPS, American PHI-5702) and transmission electron microscopy (TEM, JEM-2010). The piezoresponse force microscopy (PFM) measurements were carried out using a commercial AFM system (Park NX10, Park systems) with conductive Pt/Si-coated probes (PPP-EFM, Nanosensors).

2.3 Transferring the α-GeTe nanosheets on SiO_2/Si substrate

The as-grown α-GeTe nanosheets were transferred from mica onto Au/SiO_2/Si substrate by a wet transfer process with the help of polymethyl methacrylate (PMMA). The PMMA solution was spin-coated (at 3000 rpm for 30 s) on the mica substrates with α-GeTe. PMMA/mica was baked at 60 °C for 30 min. Subsequently, the PMMA/mica film was detached from the mica substrate and captured by the Au/SiO_2/Si substrate, followed by heating at 85 °C for 60 min. Finally, PPMA was dissolved in hot anisole, and α-GeTe nanosheets were successfully transferred to Au coated on a SiO_2/Si or copper mesh.

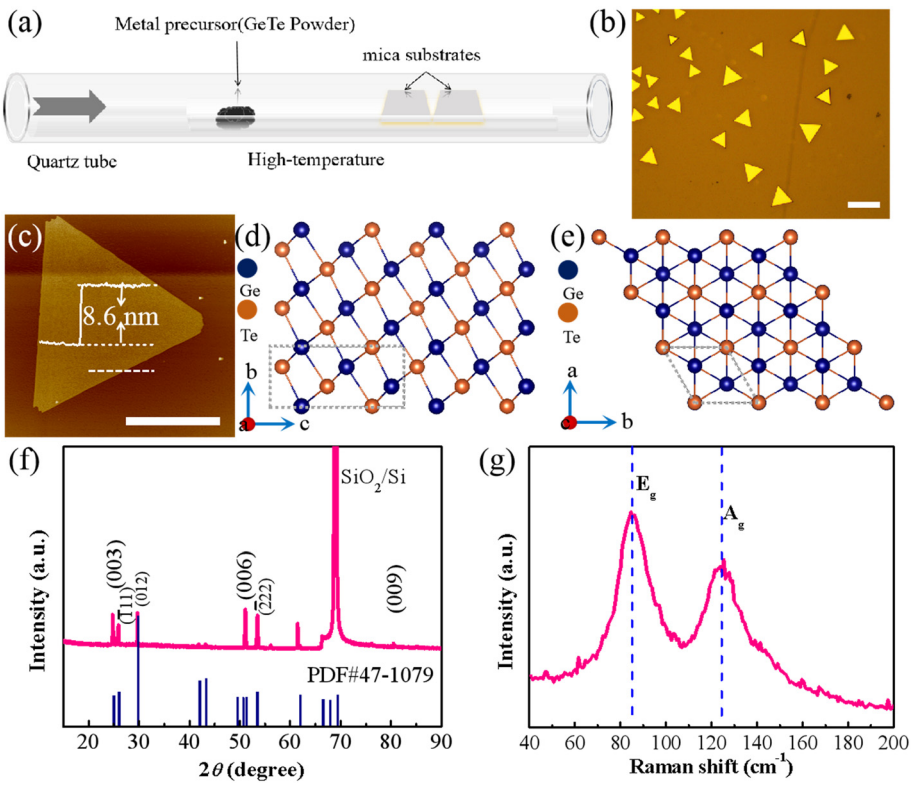

Fig. 1 (a) Schematic of the CVD setup. (b) OM image of the as-grown α-GeTe nanosheets, scale bar: 20 μm. (c) AFM image of α-GeTe nanosheets with a thickness of 8.6 nm, scale bar: 5 μm. (d) Side view and (e) top view structure of the α-GeTe crystal. (f) XRD patterns of α-GeTe nanosheets. (g) Raman spectra of α-GeTe nanosheets.

Published on 11 July 2024. Downloaded on 11/19/2024 1:20:51 PM.

3. Results and discussion

α-GeTe nanosheets were successfully synthesized *via* the APCVD method. Fig. 1(b) shows a typical OM of the α-GeTe nanosheets, which mostly exhibit a typical regular triangular shape and a lateral size of up to 15 μm. The α-GeTe nanosheets show highly uniform color under a bright-field optical microscope. Fig. 1(c) shows the AFM image and corresponding height image of a typical α-GeTe nanosheets with a thickness of 8.6 nm. The three phases of GeTe are always intermingled with each other. Fig. 1(d) and (e) show the side and top views, respectively, of α-GeTe, which has a rhombohedral structure (space group, *R*3*m*)[24] with lattice parameters of a = 4.156 Å and c = 10.663 Å.[25] In α-GeTe, Ge atoms are connected with Te atoms forming covalent bonds, and six-membered rings are formed with Ge atoms and Te atoms arranged alternately.[26,27] In β-GeTe,[27–32] an octahedron is formed with the same bond length between Ge and six Te atoms (Fig. S1a and b†). In order to confirm the phases of the as-grown GeTe nanosheets, the as-grown GeTe nanosheets were transferred from the mica substrate to the SiO_2/Si substrate, and XRD analysis was used to determine the crystal structure of the GeTe nanosheets. As shown in Fig. 1(f), three main diffraction peaks corresponding to the (003), (006) and (009) planes of the XRD patterns are consistent with those from a previous study. Obviously, all prominent XRD diffraction peaks are indexed to the {00*l*} family planes, suggesting that the *c*-axis of the α-GeTe nanosheets is perpendicular to the substrate. Similarly, the XRD results (Fig. S2†) of the α-GeTe nanosheets grown on the annealed mica substrates confirmed that the resulting α-GeTe nanosheets are high-quality single crystals. The related phonon vibrational modes of α-GeTe nanosheets were confirmed by subsequent Raman spectroscopy.

Fig. 1(g) shows the Raman spectra of the 19 nm GeTe nanosheet with two characteristic peaks at 84.6 cm^{-1} and 124.5 cm^{-1}, corresponding to E_g and A_g vibration modes, respectively.[24,27,33–35] The corresponding AFM image is shown in Fig. S3.†

In addition to determining the composition and chemical state, α-GeTe nanosheets were further characterized by XPS. Fig. S4† displays the wide-scan XPS spectrum of α-GeTe nanosheets, revealing peaks from the mica substrate and different valence states of Ge and Te. The XPS spectra and peaks of GeTe nanosheets are shown in Fig. 2, showing the obvious spectra of Ge 2p, Ge 3d and Te 3d orbits. The Ge 2p core level mainly consists of Ge $2p_{3/2}$ (1220.45 eV) and Ge $2p_{1/2}$ (1251.56 eV), as shown in Fig. 2a.[36–39] The binding energy corresponding to ~1219.5 eV is represented as a Ge^{2+} compound (Ge–Te),[39–41] while the binding energy corresponding to ~1221 eV is represented as a Ge^{4+} oxide (GeO_2).[37–39] Similarly, the binding energy at 1250.8 eV represents the Ge^{2+} compound,[38] while the corresponding binding energy at 1251.9 eV represents the Ge^{4+} oxide (GeO_2).[37,39] The Ge 3d peaks at 30.21 and 32.72 eV indicate the presence of Ge.[41,42] Similarly, Te $3d_{5/2}$ and $3d_{3/2}$ binding energies located at 577.13 eV and 587.82 eV are most likely due to TeO_2.[34,41] The anticipated Te^{2+} was detected with its distinctive paired peaks of Te $3d_{5/2}$ and $3d_{3/2}$ signals at 573.24 eV and 583.68 eV, respectively (Fig. 2c).[34,41,42] Furthermore, the morphology, atomic ratio and element distribution of the nanosheets were characterized by SEM equipped with EDS and TEM.

Fig. 3(a) and (b) shows the SEM images of α-GeTe nanosheets transferred onto the SiO_2/Si substrate, which mostly exhibit a triangular shape. The EDS result of α-GeTe nanosheets in Fig. 3(c) shows only Ge and Te elements, whose atomic ratio is close to 1 : 1, which is consistent with the expected stoichiometric ratio. Furthermore, the EDS elemental mapping of Ge, Te and Ge + Te elements, as shown in Fig. 3(d)–(f), showed that they were uniformly distributed without apparent separation. TEM was also applied to determine the crystallinity and structure of GeTe nanosheets. Fig. 3(g) shows a low-magnification plan-view TEM image of a hexagonal GeTe nanosheet. It can be observed that the surface of the nanosheets is smooth. The HR-TEM image in Fig. 3(h) shows a periodic atomic arrangement with the lattice of the α-GeTe nanosheet. The calculated lattice spacings (0.207 nm) were indexed to the (110) plane of hexagonal α-GeTe.[18,27] The lattice space was measured from SAED, as shown in Fig. 3(i), which is in good accordance with the data shown in Fig. 3(h). To fabricate large-scale 2D α-GeTe nanosheets, we presented detailed systematic studies to investigate the effect of substrate pre-annealing and

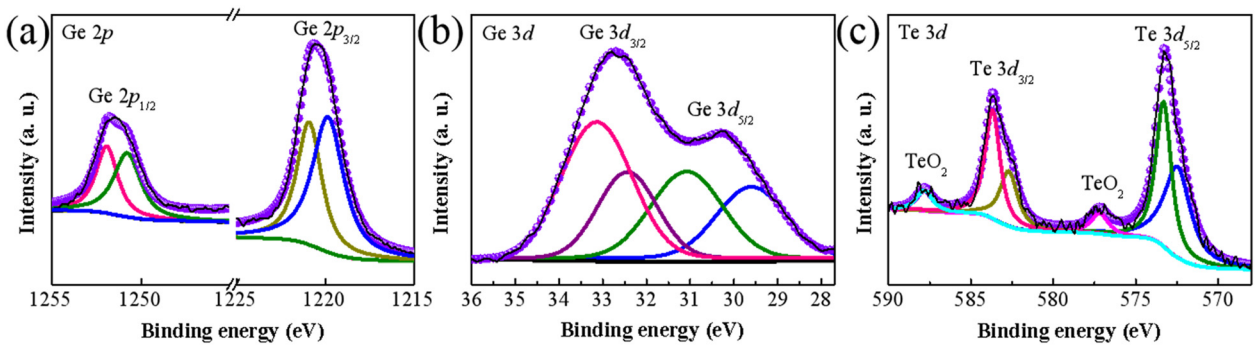

Fig. 2 Spectra of Ge 2p (a), Ge 3d (b) and Te 3d (c) orbits recorded with a photon energy of the GeTe nanosheets.

 This journal is © The Royal Society of Chemistry 2024

Published on 11 July 2024. Downloaded on 11/19/2024 1:20:51 PM.

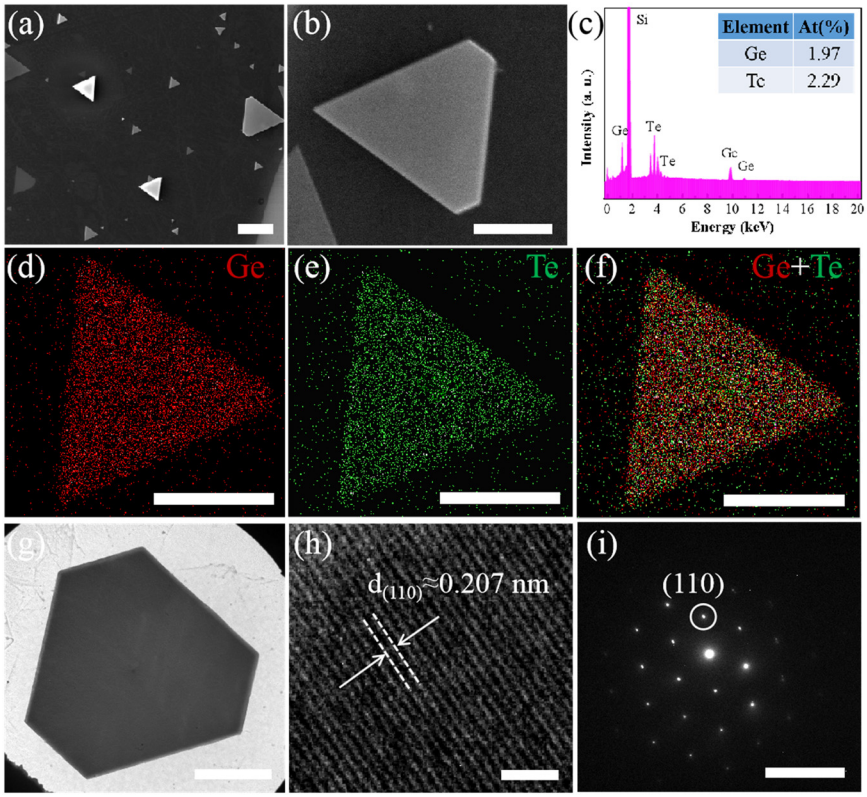

Fig. 3 (a) and (b) SEM image of α-GeTe nanosheets, scale bar: 5 μm. EDS spectrum of α-GeTe nanosheets (c) and the corresponding EDS elemental mapping images of (d) Ge, (e) Te and (f) Ge + Te, scale bar: 5 μm. (g) Low-magnification TEM image of α-GeTe nanosheets, scale bar: 5 μm. (h) HRTEM image of α-GeTe nanosheets, scale bar: 1 nm. (i) SAED images of α-GeTe nanosheets, scale bar: 5 1/nm.

growth duration. The results show that these growth parameters can be applied to control the lateral size, nucleation density and thickness of the samples. It is found that the air-annealing of the mica substrate can boost the growth of GeTe nanosheets with larger lateral sizes. The mica with a layered structure is a suitable substrate for epitaxy growth due to the dangling bond-free surface.[42,43] The mica substrate is composed of the aluminosilicate layer and K^+

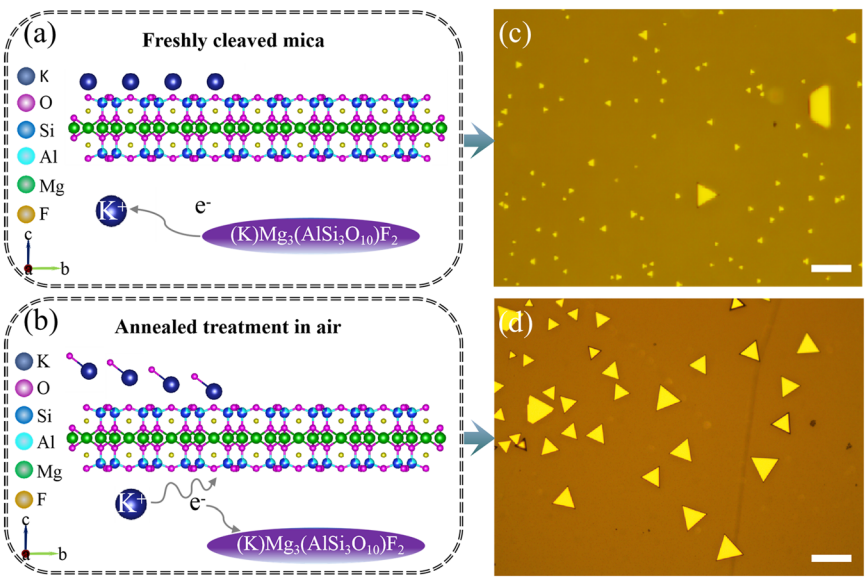

Fig. 4 (a) Schematic of freshly cleaved mica. (b) Schematic diagram of mica substrate after thermal annealing in air. OM images of α-GeTe nanosheets grown on unannealed mica (c) and annealed mica (d).

Published on 11 July 2024. Downloaded on 11/19/2024 1:20:51 PM.

ions intercalated layers.[43] As shown in Fig. 4(a), the aluminosilicate layer of the mica substrate is bound together by a layer of K^+ ions. In general, freshly cleared mica was used to fabricate 2D materials, and the K^+ ions were left on the surface of the newly dissociated mica. The randomly distributed K^+ ions, distributed on the surface of the mica substrate adsorb electrons on the surface.[32,44] According to the previous reports, the residual K^+ ions significantly affect the nucleation and growth of nanosheets.[45,46] By thermal annealing of the as-cleaved mica, the distribution of K^+ ions on the surface was altered.[44] As a result, we can modify the distribution of K^+ ions on the surface illustrated in Fig. 3(b), which leads to the growth of GeTe modification. In this work, we annealed the as-cleaved mica in the air at 500 °C for 60 minutes before the growth of α-GeTe.

For comparison, we fabricated the α-GeTe nanosheets under the same growth condition (growth temperature: 600 °C, growth duration: 10 min, 200 sccm Ar gas) on as-cleaved mica and annealed mica. As shown in Fig. 4(a)–(d), α-GeTe nanosheets grown on the as-cleaved mica showed a high nucleation density with a small lateral size, whereas low nucleation density was on the annealed mica substrate. It can be found that the lateral size of α-GeTe was significantly increased by pre-annealing of the substrate. Stephens *et al.* reported that K^+ ions on the surface of air-cleaved mica can form K_2CO_3 nanoparticles,[46] which could serve as nucleation sites for the growth of nanosheets. After air thermal annealing, residual K^+ ions may have been partially removed.[44] In other words, the role of air-annealing is to reduce the nucleation sites on the mica substrate. As a result, the pre-annealing of the substrate results in a reduction of nucleation sites and thus enhances the lateral growth of GeTe nanosheets. Furthermore, we systematically investigated the role of growth time on the lateral size of α-GeTe. Fig. 5 shows the OM images of α-GeTe nanosheets synthesized at different growth times on freshly cleaved mica (Fig. 5a–c) and annealed mica (Fig. 5d–f). When the nanosheets are grown on freshly cleaved mica, the nucleation density of α-GeTe decreases with increasing growth time, while the lateral size of the nanosheets increases with the growth time.

However, at a growth time of 5 min, the lateral size of the nanosheets is small (approximately 2–3 μm), and some GeTe particles in an incomplete nucleation state are observed (Fig. 5a). When the growth time is increased to 15 min, the lateral size of the samples can reach around 6–9 μm (Fig. 5h). Similarly, in the case of annealed mica, the morphology of the grown α-GeTe nanosheets undergoes significant changes, with the lateral size of the triangular nanosheets reaching approximately 30 μm (Fig. 5e). Moreover, when the growth time was 5 min, the lateral size of α-GeTe nanosheets could reach about 10 μm (close to the α-GeTe nanosheets grown on unannealed-mica substrates). The nanosheets with the highest nucleation density and uniform lateral size can be obtained when the growth time is 10 min.

In the recent report,[47] mica family minerals are reported to also show ferroelectric properties. In order to characterize the ferroelectric properties of α-GeTe nanosheets and eliminate the effect of mica substrate, the α-GeTe nanosheets were transferred onto conductive Au coated on SiO_2/Si for PFM measurements. Meanwhile, the Au/SiO_2/Si substrate is profitable for obtaining ferroelectric signals. Fig. 6(a) shows a schematic diagram of the PFM measurement. The conductive gold layer on SiO_2/Si was grounded, which can prevent the high current density from damaging the sample. Fig. 6(b) shows the AFM image of α-GeTe nanosheets, which was used for PFM measurement. The PFM phase and amplitude

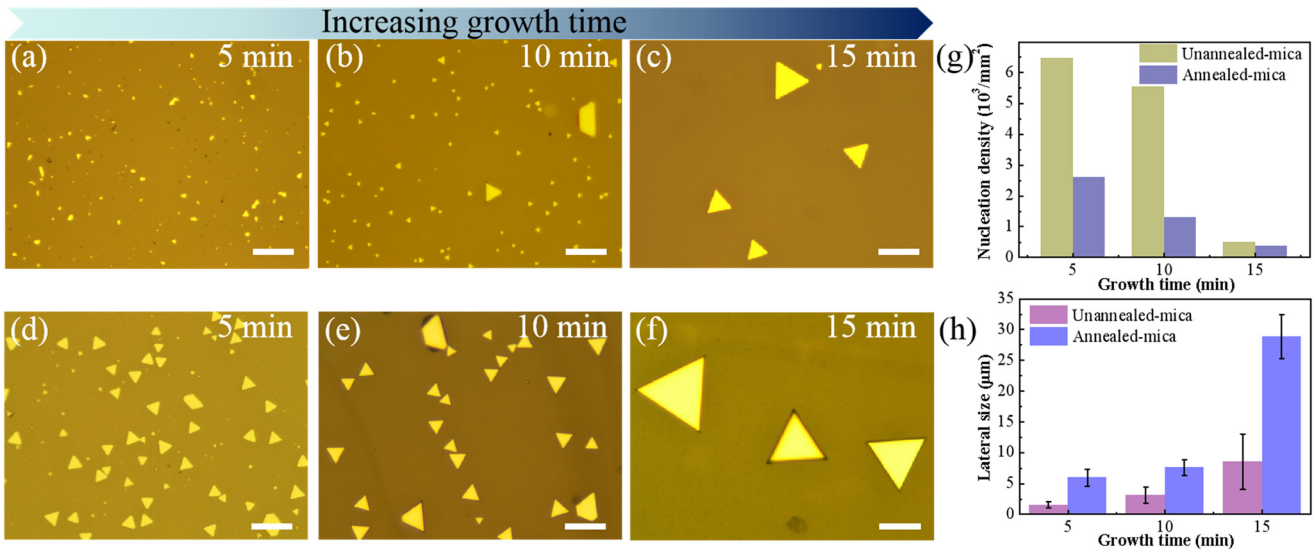

Fig. 5 OM images of α-GeTe nanosheets at different growth times on unannealed-mica (a–c) and annealed-mica (d–f) substrates. The scale bars are 20 μm. (g) Nucleation density changes with the growth time. (h) Lateral size of nanosheets changes with the growth time.

 This journal is © The Royal Society of Chemistry 2024

Published on 11 July 2024. Downloaded on 11/19/2024 1:20:51 PM.

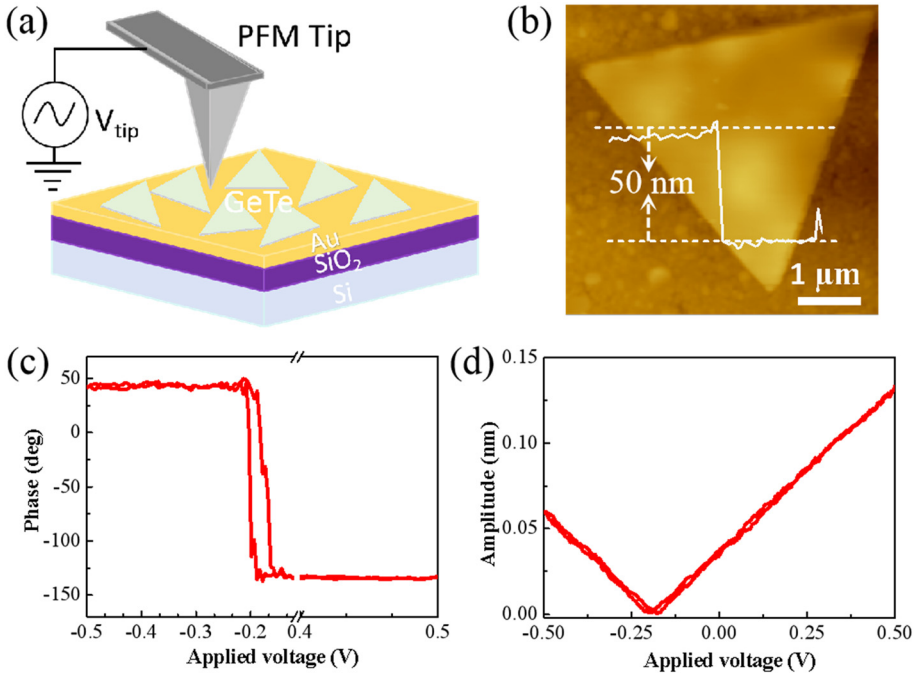

Fig. 6 (a) Schematic diagram of the PFM measurement. (b) Topography image and height profile of 50 nm α-GeTe nanosheets on the conductive substrate. PFM phase (c) and amplitude (d) hysteresis loops of the corresponding 50 nm α-GeTe nanosheets scanned by DC triangular waveform.

hysteresis loops of the corresponding 50 nm α-GeTe are shown in Fig. 6(c). The applied voltage was scanned by a triangular waveform from −0.5 to 0.5 V. The off-field phase hysteresis loop clearly shows two discrete polarization states with ~180° phase difference and an asymmetric butterfly loop was observed in the amplitude signal, which is consistent with the switching voltage of the ferroelectric polarization. Furthermore, to further verify the correctness of ferroelectric signals. The measurements were repeated several times at different selected regions of the same α-GeTe nanosheets and nearly identical responses were obtained. These results indicate that 2D α-GeTe nanosheets possess a stable room-temperature ferroelectric polarization.

4. Conclusions

In conclusion, we have successfully synthesized large single-crystal GeTe nanosheets by APCVD on mica substrates. The distribution of K^+ ions on the surface of as-cleaved mica was altered by thermal annealing. As a result, thermal annealing is an effective way to control the nucleation of GeTe and enhance the lateral size of α-GeTe nanosheets. Meanwhile, the grown single-crystal α-GeTe nanosheets in this study exhibits a lateral size of up to ≈30 μm and a thickness as low as ≈8.6 nm. Both XRD and Raman spectra show the GeTe nanosheets are high-quality single crystals with α phase. Furthermore, the ferroelectric properties of α-GeTe nanosheets were investigated through PFM. To the best of our knowledge, the ferroelectric characteristics of α-GeTe nanosheets grown by CVD are reported for the first time, which show novel opportunities in the fundamental research of 2D ferroelectric materials.

Data availability

The authors confirm that the data supporting the findings of this study are available within the article and its ESI.†

Conflicts of interest

There are no conflicts to declare.

Acknowledgements

This project was supported by the National Natural Science Foundation of China (NSFC) (No. 12374200), the Ministry of Science and Technology (MOST) of China (No. 2023YFA1406500), the Strategic Priority Research Program and Key Research Program of Frontier Sciences (Chinese Academy of Sciences, CAS) (No. XDB30000000, No. QYZDB-SSW-SYS031), and the Fundamental Research Funds for the Central Universities and the Research Funds of Renmin University of China (No. 21XNLG27 and 22XNH097).

References

1 L. Li, Z. Chen, Y. Hu, X. Wang, T. Zhang, W. Chen and Q. Wang, *J. Am. Chem. Soc.*, 2013, **135**, 1213–1216.
2 A. V. Kolobbov, P. Fons, J. Tominaga, A. I. Frenkel, A. L. Ankudinov, S. N. Yannopoulos, K. S. Andrikopoulos and T. Uuga, *Jpn. J. Appl. Phys.*, 2005, **44**, 3345–3349.

Published on 11 July 2024. Downloaded on 11/19/2024 1:20:51 PM.

3 S. Raoux, H.-Y. Cheng, M. A. Caldwell and H.-S. P. Wong, *Appl. Phys. Lett.*, 2009, **95**, 71910.
4 G. Bruns, P. Merkelbach, C. Schlockermann, M. Salinga, M. Wuttig, T. D. Happ, J. B. Philipp and M. Kund, *Appl. Phys. Lett.*, 2009, **95**, 43108.
5 C. Wood, *Rep. Prog. Phys.*, 1999, **51**, 459–539.
6 D. Wu, L.-D. Zhao, S. Hao, Q. Jiang, F. Zheng, J. W. Doak, H. Wu, H. Chi, Y. Gelbstein, C. Uher, C. Wolverton, M. Kanatzidis and J. He, *J. Am. Chem. Soc.*, 2014, **136**, 11412–11419.
7 M. Hong and Z. G. Chen, *Acc. Chem. Res.*, 2022, **55**, 3178–3190.
8 D. Di Sante, P. Barone, R. Bertacco and S. Picozzi, *Adv. Mater.*, 2013, **25**, 509–513.
9 M. Liebmann, C. Rinaldi, D. Di Sante, J. Kellner, C. Pauly, R. N. Wang, J. E. Boschker, A. Giussani, S. Bertoli, M. Cantoni, L. Baldrati, M. Asa, I. Vobornik, G. Panaccione, D. Marchenko, J. Sánchez-Barriga, O. Rader, R. Calarco, S. Picozzi, R. Bertacco and M. Morgenstern, *Adv. Mater.*, 2016, **28**, 560–565.
10 H. J. Elmers, R. Wallauer, M. Liebmann, J. Kellner, M. Morgenstern, R. N. Wang, J. E. Boschker, R. Calarco, J. Sánchez-Barriga, O. Rader, D. Kutnyakhov, S. V. Chernov, K. Medjanik, C. Tusche, M. Ellguth, H. Volfova, S. Borek, J. Braun, J. Minár, H. Ebert and G. Schönhense, *Phys. Rev. B*, 2016, **94**, 201403.
11 J. J. Gervacio-Arciniega, E. Prokhorov, F. J. Espinoza-Beltrán and G. Trapaga, *J. Appl. Phys.*, 2012, **112**, 52018.
12 M. J. Polking, M.-G. Han, A. Yourdkhani, V. Petkov, C. F. Kisielowski, V. V. Volkov, Y. Zhu, G. Caruntu, A. P. Alivisatos and R. Ramesh, *Nat. Mater.*, 2012, **11**, 700–709.
13 A. V. Kolobov, D. J. Kim, A. Giussani, P. Fons, J. Tominaga, R. Calarco and A. Gruverman, *APL Mater.*, 2014, **2**, 66101.
14 C. Cui, F. Xue, H. Wei-Jin and L. Lain-Jong, *npj 2D Mater. Appl.*, 2018, **2**, 18.
15 Y. Zhang, W. Jie, P. Chen, W. Liu and J. Hao, *Adv. Mater.*, 2018, **30**, 1707007.
16 D. S. Jeong, R. Thomas, R. S. Katiyar, J. F. Scott, H. Kohlstedt, A. Petraru and C. S. Hwang, *Rep. Prog. Phys.*, 2012, **75**, 076502.
17 J. Wang, X. Xu, T. Cheng, L. Gu, R. Qiao, Z. Liang, D. Ding, H. Hong, P. Zheng, Z. Zhang, Z. Zhang, S. Zhang, G. Cui, C. Chang, C. Huang, J. Qi, J. Liang, C. Liu, Y. Zuo, G. Xue, X. Fang, J. Tian, M. Wu, Y. Guo and K. Liu, *Nat. Nanotechnol.*, 2022, **17**, 33–38.
18 Y. Yao, X. Zhan, C. Ding, F. Wang, Y. Wang, J. Yang, Z. Wang and J. He, *Nano Res.*, 2022, **15**, 6736–6742.
19 F. Tong, J. D. Liu, X. M. Cheng, J. H. Hao, G. Y. Gao, H. Tong and X. S. Miao, *Thin Solid Films*, 2014, **568**, 70–73.
20 Y. Zhang, J. Shi, G. Han, M. Li, Q. Ji, D. Ma, Y. Zhang, C. Li, X. Lang, Y. Zhang and Z. Liu, *Nano Res.*, 2015, **8**, 2881–2890.
21 Y. Zhang, Y. Zhang, Q. Ji, J. Ju, H. Yuan, J. Shi, T. Gao, D. Ma, M. Liu, Y. Chen, X. Song, H. Y. Hwang, Y. Cui and Z. Liu, *ACS Nano*, 2013, **7**, 8963–8971.
22 X. Xu, Z. Zhang, L. Qiu, J. Zhuang, L. Zhang, H. Wang, C. Liao, H. Song, R. Qiao, P. Gao, Z. Hu, L. Liao, Z. Liao, D. Yu, E. Wang, F. Ding, H. Peng and K. Liu, *Nat. Nanotechnol.*, 2016, **11**, 930–935.
23 M. Wang, M. Huang, D. Luo, Y. Li, M. Choe, W. K. Seong, M. Kim, S. Jin, M. Wang, S. Chatterjee, Y. Kwon, Z. Lee and R. S. Ruoff, *Nature*, 2021, **596**, 519–524.
24 H. Min, Z. Jin and C. Zhi Gang, *Adv. Mater.*, 2019, **31**, 1807071.
25 W. G. Zeier, A. Zevalkink, Z. M. Gibbs, G. Hautier, M. G. Kanatzidis and G. J. Snyder, *Angew. Chem., Int. Ed.*, 2016, **55**, 6826.
26 L. M. Schoop, L. Müchler, C. Felser and R. J. Cava, *Inorg. Chem.*, 2013, **52**, 5479.
27 W. Li, R. Wu, Q. Li, Q. Tao, M. Z. Saeed, X. Li, S. Wan, R. Song, D. Shen, K. Huang, M. Liu, B. Li, B. Zhao, J. Liu, Y. Liu, B. Li, J. Li and X. Duan, *Adv. Funct. Mater.*, 2022, **32**, 2201673.
28 M. Miao, J. Brgoch, A. Krishnapriyan, A. Goldman, J. A. Kurzman and R. Seshadri, *Inorg. Chem.*, 2013, **52**, 8183–8189.
29 B. B. Van Aken, T. T. M. Palstra, A. Filippetti and N. A. Spaldin, *Nat. Mater.*, 2004, **3**, 164–170.
30 N. A. Spaldin, S.-W. Cheong and R. Ramesh, *Phys. Today*, 2010, **63**, 38–43.
31 Z. Wang, Y. Xie, H. Wang, R. Wu, T. Nan, Y. Zhan, J. Sun, T. Jiang, Y. Zhao and Y. Lei, *Nanotechnology*, 2017, **28**, 325602.
32 K. S. Andrikopoulos, S. N. Yannopoulos, G. A. Voyiatzis, A. V. Kolobov, M. Ribes and J. Tominaga, *J. Phys.: Condens. Matter*, 2006, **18**, 965–979, DOI: **10.1088/0953-8984/18/3/014**.
33 K. S. Andrikopoulos, S. N. Yannopoulos, A. V. Kolobov and J. Tominaga, *J. Phys. Chem. Solids*, 2007, **68**, 1074–1078.
34 Y. Zhao, L. Tang, S. Yang, S. P. Lau and K. S. Teng, *Nanoscale Res. Lett.*, 2020, **15**, 138.
35 D.-J. Xue, F. Jiao, H.-J. Yan, W. Xu, D. Zhu, Y.-G. Guo and L.-J. Wan, *Chem. – Asian J.*, 2013, **8**, 2383–2387.
36 A. S. Almuslem, A. N. Hanna, T. Yapici, N. Wehbe, E. M. Diallo, A. T. Kutbee, R. R. Bahabry and M. M. Hussain, *Appl. Phys. Lett.*, 2017, **110**, 074103.
37 P. Harshawardhan, A. V. Kir'Yanov, A. D. Shyamaldas, D. D. Mrinmaypal, Y. O. Barmenkov, J. A. Minguella-Gallardo, S. K. Bhadra and M. C. Paul, *Appl. Opt.*, 2017, **56**, 9315.
38 N. M. Lyadov, S. M. Khantimerov, I. V. Yanilkin, I. A. Faizrakhmanov, V. V. Bazarov, V. F. Valeev, N. M. Suleimanov, K. Kierzek and T. P. Gavrilova, *J. Phys.: Conf. Ser.*, 2020, **1588**, 012024.
39 S. Z. Rahaman, S. Maikap, S. K. Ray, H.-Y. Lee, W. Chen, F. T. Chen, M. Kao and M. Tsai, *Jpn. J. Appl. Phys.*, 2012, **51**, 04DD11.
40 H. Qian, H. Tong, L. J. Zhou, B. H. Yan, H. K. Ji, K. H. Xue, X. M. Cheng and X. S. Miao, *J. Phys. D: Appl. Phys.*, 2016, **49**, 495302.
41 A. N. D. Kolb, N. Bernier, E. Robin, A. Benayad, J. L. Rouvière, C. Sabbione, F. Hippert and P. Noé, *ACS Appl. Electron. Mater.*, 2019, **5**, 701–710.

 This journal is © The Royal Society of Chemistry 2024

42 Q. Ji, Y. Zhang, T. Gao, Y. Zhang, D. Ma, M. Liu, Y. Chen, X. Qiao, P.-H. Tan, M. Kan, J. Feng, Q. Sun and Z. Liu, *Nano Lett.*, 2013, **13**, 3870–3877.
43 H. K. Christenson and N. H. Thomson, *Surf. Sci. Rep.*, 2016, **71**, 367–390.
44 M.-H. Chiu, X. Ji, T. Zhang, N. Mao, Y. Luo, C. Shi, X. Zheng, H. Liu, Y. Han, W. L. Wilson, Z. Luo, V. Tung and J. Kong, *Adv. Electron. Mater.*, 2023, 2201031.
45 Y. Min, Y. Bitla and C. Ying-Hao, *Mater. Chem. Phys.*, 2019, **234**, 85–195.
46 C. J. Stephens, Y. Mouhamad, F. C. Meldrum and H. K. Christenson, *Cryst. Growth Des.*, 2010, **10**, 734–738.
47 Z. Huang, Z. Zhang, R. Zhang, B. Ding, L. Yang, K. Wu, Y. Xu, G. Zhong, C. Ren, J. Liu, Y. Hao, M. Wu, T. Ma and B. Liu, *Natl. Sci. Rev.*, 2024, **11**, nwae108.

Published on 11 July 2024. Downloaded on 11/19/2024 1:20:51 PM.